

Application of Distributed Fibre Optic Cables in Piles

Jakub G. Kania¹, Kenny Kataoka Sorensen² and Bengt H. Fellenius³

¹PhD student, Department of Engineering, Aarhus University, Aarhus, Denmark and cp test a/s, Vejle, Denmark

²Associate Professor, Department of Engineering, Aarhus University, Aarhus, Denmark

³Consulting Engineer, Sidney, BC, Canada, V8L 2B9

¹E-mail: jakub@cptest.dk

²E-mail: kks@eng.au.dk

³E-mail: bengt@fellenius.net

ABSTRACT: A high spatial resolution distributed fibre optic sensing system for measuring strain and temperature was used to instrument fourteen single piles subjected to general subsidence. Thirteen piles were driven (six steel and seven precast concrete) and one was a cased continuous flight auger pile, CFA. The CFA pile was subjected to a static loading test. The distributed fibre optic analyser measured the spectral shift in the fibre Rayleigh scatter to obtain strain and temperature data. The seasonal temperature changes in the surficial soil layers showed to influence the strain records. Several lessons were learnt from the application of distributed fibre optic sensors in piles, such as installation methods, influence of temperature, and performance of fibre optic cables.

KEYWORDS: Instrumented Piles, Distributed Fibre Optic Sensing, Rayleigh Scattering, Temperature Effect, Strain Gauges

1. INTRODUCTION

Instrumentation of piles are used to provide detailed information about soil-pile interaction, necessary for optimizing the design of a piled foundation, e.g., determine distribution of shaft resistance and measure the pile toe load-movement response. Conventionally, piles have been instrumented by means of telltales and strain gages placed along the pile to determine the force distribution caused by a load applied to the pile head or an axial force induced by subsiding soils. In recent years, there has been an increasing interest in the using distributed fibre optic sensing (DFOS) systems for monitoring strain in geotechnical structures. The DFOS technology employs light scattering along an optical fibre (Culshaw and Kersey 2008). Owing to the vast measurement range of the DFOS (tens of kilometres), they were primarily used for pipeline monitoring projects (Inaudi and Glisic 2010, Ravet et al. 2017). The development in fibre optic analysers, mainly in terms of spatial resolution and accuracy, allowed to use the technology also in geotechnical applications, e.g., tunnels (Mohamad et al. 2010), slopes (Nöther et al. 2008), and piles (Klar et al. 2006, Kechavarzi et al. 2019, Pelecanos et al. 2018). Most of the early studies employed Brillouin-based DFOS systems, whereas Rayleigh-based DFOS systems in piles has received little attention (Monsberger et al. 2016, Bersan et al. 2018).

This paper focuses on lessons learnt from employing a Rayleigh-based DFOS system to monitor strain in piles, describing the components of the DFOS system and methods of installing distributed fibre optic (FO) cables in piles, as well as presenting method of analysis of the records, and observed performance.

2. DISTRIBUTED FIBRE OPTIC ANALYSER AND CABLES

A DFOS system is composed of two main elements: a fibre optic spectrum analyser and an FO cable. The subject study of measuring strain and temperature changes in piles, a Luna ODiSI-B system was used. The system comprises an interrogation unit (IU), a stand-off cable, and a remote module (see Figure 1). The IU uses swept-wavelength interferometry to measure the spectral shift in the Rayleigh backscatter (Luna 2017). The maximum sensing length of the unit employed in the subject test was 20 m and the spatial and sampling resolutions were 5.2 and 2.6 mm, respectively. The spatial resolution is a length over which the IU calculates a single strain or temperature data point. The sampling resolution is the distance between two data points. FO cable sensors, standard telecommunication bare fibres or commercially available coated strain and temperature sensing cables can be used. The subject study

employed a FO cable connected to the IU through the remote module and stand-off cable.



Figure 1 ODiSI-B measurement system (Luna 2017)

Figure 2(a) shows a bare fibre glued to the reinforcement bar and Figure 2(b) shows FO strain and temperature cables attached to the reinforcement cage. The FO strain cable must transfer the applied strain without any slippage between the coatings. Thus, bare fibres would appear to be most suitable. However, bare cables are brittle and unsuitable in a harsh environment, such as a pile. Therefore, strain sensing cables with a coating to serve as a protection layer have been developed. It is important that the coating and any glue (epoxy) for affixing the sensor to a construction unit is free of shrinkage and creep to avoid imposing extraneous strain in the cable. In contrast to the FO strain cable, the FO temperature cable should allow slippage between the protective layers to eliminate all strain influencing the temperature records. In this study, a BRUsens V9 strain cable and a BRUsens temperature 85°C cable were used.

The IU used in this study requires a distributed FO cable to have an LC/APC connector to connect the sensor to the IU (through a remote unit and stand-off cable). The fibre-end termination should ensure a greater than -65dB return loss (no back reflection). This can be achieved by splicing a coreless fibre or a commercially available no-reflection terminator to the fibre end. An alternative method is to terminate the fibre with a few (5 to 6) small diameter (about 2 mm) loops. In this study, the termination was made by making small diameter loops.

In using an IU type Luna ODiSI-B, each FO cable must have a sensor key (Luna 2017). The sensor key is a file containing the

characteristic spectral shift for a given FO cable and is used for its identification. The unit is using an algorithm along the first 200 mm of the connected sensor to identify it (Luna 2017). Therefore, it is important to relieve this part of the FO sensor from any strain and temperature gradients. This can be done by placing a protective tube or shaping the fibre into a loop along this part. If a FO sensor is damaged, and repaired, or not identified by the IU, all its characteristics must be re-keyed, i.e., sensor name, strain, temperature coefficients, and start and end locations of the sensing section along the fibre.

To validate the re-keying procedure, an identified FO sensor was re-keyed. The standard deviation between strain measurement obtained from identified and re-keyed sensor was $\pm 2 \mu\epsilon$. The sensor key can be provided by the manufacturer of the unit or can be created by the user.

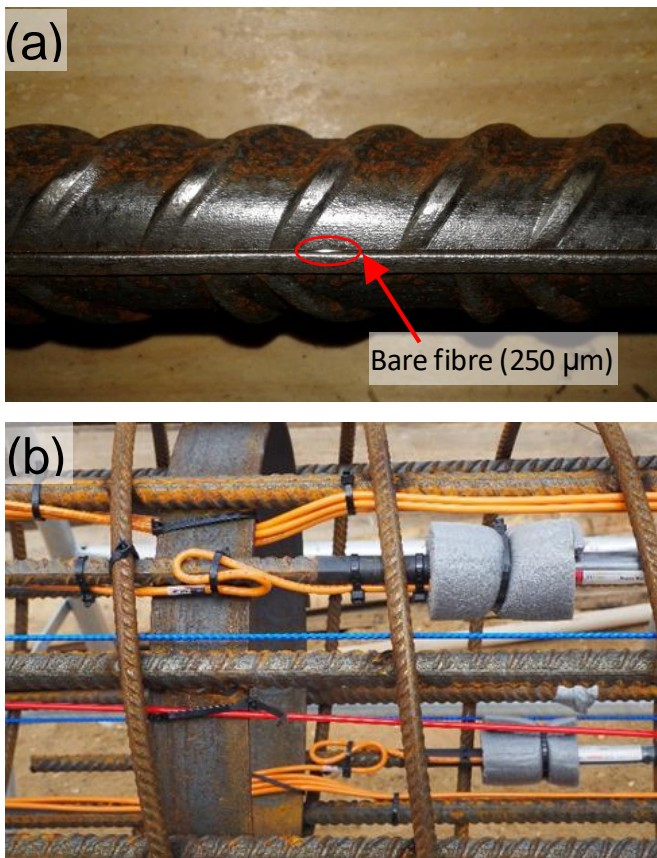


Figure 2 An example of (a) a bare fibre glued to the reinforcement bar along the longitudinal rib and (b) FO strain (blue) and temperature (red) cables attached to the reinforcement cage. The "250 µm" label refers to the thickness of the fibre cable

The IU records spectral shift in the fibre. This shift (frequency or wavelength) is proportional to change of temperature or strain in proportion to the properties of the fibre as calibrated in the laboratory for response to frequency shift for a known temperature or strain change (Kreger et al. 2006, Monsberger et al. 2016). For standard telecommunication fibres the value of the coefficients may vary around 10 % (Luna 2017). In this study, the temperature and strain coefficients of $0.634 \text{ }^\circ\text{C}/\text{GHz}$ and $-6.67 \mu\epsilon/\text{GHz}$ were used, respectively.

According to the manufacturer, the accuracy of the IU used in this study was $\pm 25 \mu\epsilon$ (Luna 2017). The measurements were compared to NIST traceable extensometer measurements measuring over the range of 0 to 10,000 $\mu\epsilon$. An accuracy of 0.25 % is similar to the accuracy of commercially available vibrating wire (VW) strain gages.

According to the VW data sheet (from Geosense) the accuracy of VW gauges is 0.1-0.5% FS (where the FS is 3000 $\mu\epsilon$).

3. INSTALLATION OF FIBRE OPTIC CABLES IN PILES

A distributed FO cable usually combines two sections; one for sensing and one for routing. The sensing section provides strain or temperature data. The routing section links the sensing section with the IU (Kechavarzi et al. 2016). A robust FO cable should be used as routing section, since it is placed outside the monitored structure. The two sections are connected by a fusion splice or by a fibre optic adapter. The former entails lower optical loss than the latter, but safe fusion splicing could be difficult to achieve on site. Either connection is likely the weakest spot of the distributed FO cable. Therefore, it should be well protected. One method of protection is to keep them outside the monitored element, e.g., in a protective box or sleeve. Another is to embed them in the monitored element. The advantage of placing them outside is the accessibility to repair. In this study, the connections were kept outside for the CFA pile and were embedded for the steel or precast concrete driven piles. Both methods worked well.

Figure 3 shows a typical cross-section layout of an instrumented (a) steel pile and (b) a reinforcement cage of a bored pile. It is good practice to install at least one pair of opposite mounted strain sensors, because it is very likely that the pile will be subjected to bending. Installing two pairs will ensure a back-up redundancy in case of damage to the FO cable, or provide a valuable independent verification (confirmation) of unexpected results. Because the FO system provides continuous measurements, the location of sensors with depth is not an issue.

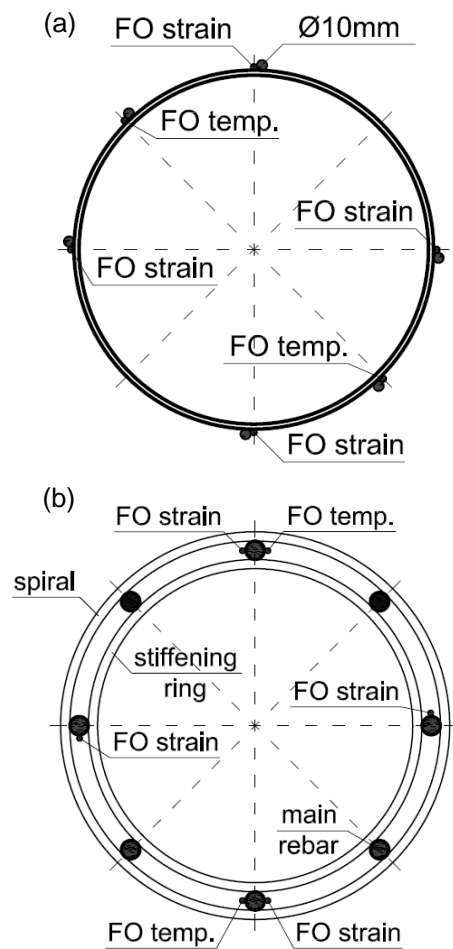


Figure 3 Typical cross-section layout of FO cables attached to (a) a steel pile and (b) a bored pile

A FO installation can either be fully bonded or installed between fixed points. In the fully bonded condition, the FO cable is continuously attached to the structure. In the fixed-point method, the FO cables provide intermittent strain information, i.e., only between the fixed points (Kechavarzi et al. 2016). In piles, the fully bonded method is preferable and the FO cables are entirely glued or embedded in the structure. Figure 4a shows an installation of a FO cable on the surface of a steel pile. An additional steel rebar was welded to the pile (one side only) as a guide and protection for the FO cable. Close to the pile toe, the bar was bent around to protect the cable end during the driving of the pile. Before attaching the FO cable to the pile, the steel surface was polished, cleaned from dust, and degreased. The FO cable was glued to the pile surface and covered using an epoxy component.

Figure 4b shows FO cables installed in a precast concrete pile. The FO cables were inserted into grooves (cleaned from dust and primed before placing the cables) and fixed with an epoxy glue. Figure 4c shows epoxy-coated FO cables installed on a reinforcement cage. The cables were installed affixed the main reinforcement bars, as shown in Figure 4d. A rubber pad was placed around each FO strain cable-tie to avoid localised point stress from cable ties. The FO temperature cables were installed without rubber pads. The cables can also be attached using specialised cable clamps (Kechavarzi et al. 2016). To avoid the flow of wet concrete affecting a FO cable, it is recommended to place the FO cables (strain and temperature) close

to the reinforcement along the whole length of the sensing section. It can be done by placing the cable ties at close spacing, e.g., at every 1.0 m. It is necessary to record strains immediately after placing in the pile (in the reinforcing cage) and before pouring the concrete, as well as after pouring because the heating and cooling involved in the hydration process will impose differential strain in the concrete and reinforcement. Such strain has no relation to the interaction between the pile and the soil and must be considered in the data analysis (Fellenius et al. 2009).

Before the FO strain cables are affixed to the structure, it is good practice to pre-tension the cable to an amount larger than the expected compressive strain (Kechavarzi et al. 2016). An example of pre-tensioning of a FO strain cable is shown in Figure 5. A pre-tensioning between two known points along the element can help align the length scale of the FO cable. Once a FO cable is attached to a structure, the locations of interest (e.g., pile head, specific depths, and pile toe) should be established, for example, by pressing or heating/cooling the FO cable at the location of interest and recording the signal at the same time.

It is important to avoid sharp bends along the FO cables to avoid loss of signal. An area where a bend easily occurs is where the cable exits from a structure. Figure 6 presents FO and VW cables exiting from a pile head. The FO cables were additionally sleeved using plastic tubes.

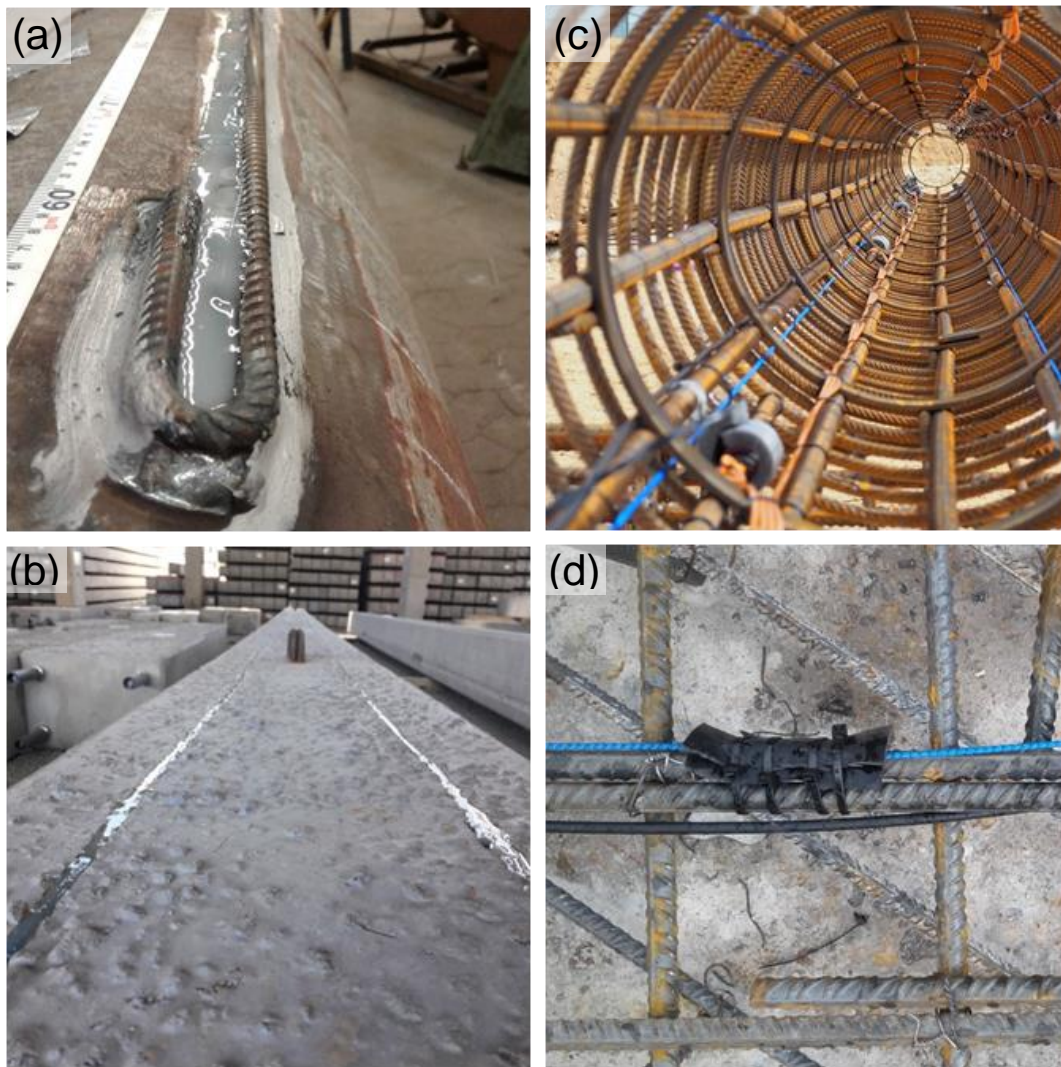


Figure 4 FO cable installation in piles: (a) glued to a steel pile, (b) glued in a groove cut along a precast concrete pile, (c) attached to a reinforcement cage, (d) attached to a rebar

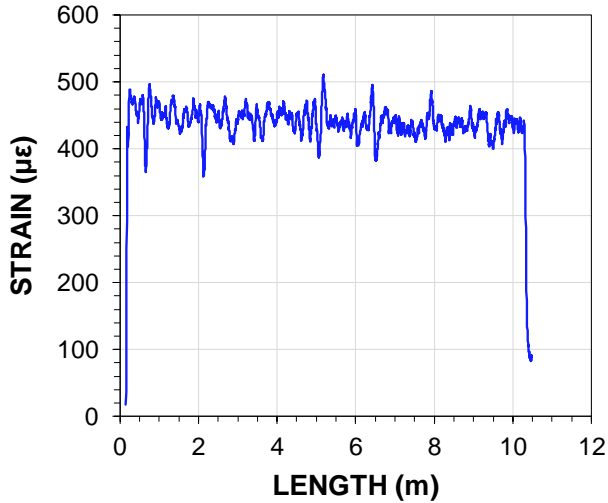


Figure 5 Pre-tension strain of a FO strain cable



Figure 6 A pile head and the sleeved FO cables at the exit points

4. DATA ANALYSIS

The measurements are always referenced to an initial state of strain (or temperature) in the cable. Therefore, it is important to establish a reliable reference reading (initial reading) to the measurements. The initial reading is actually several readings, each one taken when a change is made in the construction process from initial placement to start of a test or monitoring a development over time. Moreover, each such should be recorded over a brief period of time to eliminate any effect of a mistake or disturbance during the recording.

4.1 Influence of Temperature

The distributed FO sensors are sensitive to strain and temperature changes (Kreger et al. 2006). Thus, to obtain the mechanically induced strains the measured strains must be thermally compensated in case of any temperature changes. Because the stiffness of all the materials making up the FO cable is much smaller than the stiffness of the host structure (e.g., steel and/or concrete), it can be assumed that the FO cable undergoes the same thermal expansion as the host structure (Kechavarzi et al. 2016). However, the temperature change will still shift the spectrum of light scattered in the fibre (Luna 2014). Therefore, the thermal expansion of the host structure and the temperature effect on the scattered light in the fibre must be considered in order to obtain thermally-compensated strains. As mentioned before, strain and temperature conversion coefficients are used to convert the spectral shift into strain or temperature data.

For example, a coefficient of $1 \text{ GHz} = -0.634 \text{ }^\circ\text{C} = -6.67 \text{ } \mu\epsilon$ will show a temperature effect on the FO sensor of about $10 \text{ } \mu\epsilon/^\circ\text{C}$. The mechanical strain can be calculated using Eq. 1 (Luna 2014):

$$\epsilon_m^z = \Delta v_S^z \cdot k_\epsilon - (0,95 \cdot \Delta v_T^z \cdot k_\epsilon + \Delta v_T^z \cdot k_T \cdot \alpha_L) \quad (1)$$

where ϵ_m^z = mechanical strain at depth z
 Δv_S^z = spectral shift in a strain FO cable at depth z
 Δv_T^z = spectral shift in a temperature FO cable at depth z
 k_ϵ = strain conversion factor (strain/frequency)
 k_T = temperature conversion factor ($^\circ\text{C}/\text{frequency}$)
 α_L = thermal expansion coefficient of a monitored element

4.2 Strain Data Interpretation

The axial strain should be determined from Eq. 2 using the average of the records of a pair of strain FO cables placed at opposing diameters and at equal distance from the center of the pile.

$$\epsilon_a^z = \frac{1}{2}(\epsilon_1^z + \epsilon_2^z) \quad (2)$$

where ϵ_a^z = averaged axial mechanical strain at depth z
 ϵ_1^z and ϵ_2^z = mechanical strain of two opposite FO strain cables at depth z

The axial force can be calculated by multiplying the processed mechanical strains with the pile stiffness (EA/L , $L=1$). The stiffness of the concrete pile can be calculated using tangent or secant stiffness (Fellenius 2013; 2019).

The mechanical strain data of two opposite FO cables can be used to calculate: curvature, gradient (change of curvature), lateral displacement, bending moment, and shear force according to Eqs. 3 through 7.

$$\kappa^z = \frac{1}{d}(\epsilon_1^z - \epsilon_2^z) \quad (3)$$

$$\theta^z = \int_0^z \kappa \, dz + A \quad (4)$$

$$u^z = \int_0^z \theta \, dz + B \quad (5)$$

$$M^z = EI\kappa^z \quad (6)$$

$$Q^z = \frac{d}{dz} EI\kappa^z \quad (7)$$

where κ^z = curvature at depth z
 d = distance between two FO sensors
 θ^z = gradient at depth z
 u^z = lateral displacement at depth z
 M^z = bending moment at depth z
 E = the Young's modulus of the element
 I = moment of inertia
 Q^z = shear force at depth z
 A and B = integration coefficients as determined by the boundary conditions.

4.3 Smoothing and Filtering of Data

For the subject project, the IU was set to record five times (one record per second) and the average was determined. To smoothen the distributed fibre optic data, a moving average was then calculated. For the steel pile, the moving length was 0.26 m and for the precast piles it was 1.0 m. For a concrete pile, it is necessary to check that the moving average has not become affected by a sudden change of stiffness (cross section) or a fissure.

Figure 7 shows an example of raw and average FO strain records. Outlier data points were removed before averaging.

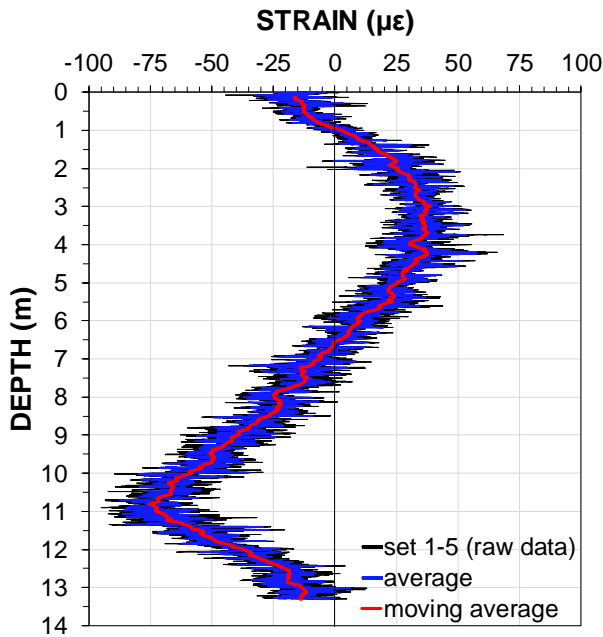


Figure 7 An example of raw and smoothed strain data obtained from an individual strain FO cable

5. PERFORMANCE OF FIBRE OPTIC CABLES IN PILES

5.1 Distribution of Strain along A Driven Steel Pile after Driving

The magnitude of strain introduced by the pile construction must be known and considered in the analysis of the strain records. Figure 8 shows the distributions of thermally corrected strain in four individual FO strain cables and the average (black line) obtained on November 13, 2017 immediately after driving a 11.5 m long 273-mm diameter, closed-toe steel pile. Negative values denote compression. One individual FO cable (S0013) reported a compression peak at 9.0 m depth, whereas its companion (S0011) did not show a similar peak. The records of this pair were removed from the average of the two pairs over the length between 8.8 through 9.4 m depth.

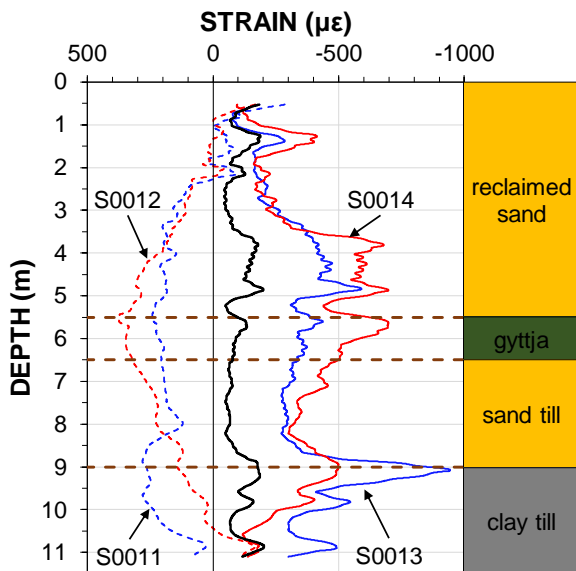


Figure 8 Distribution of strains along individual strain FO cables mounted on a driven steel pile

5.2 Performance of FO Strain Cables in Concrete Piles

5.2.1 Influence of non-uniform concrete pile stiffness

Figure 9 shows the strain distributions from an individual strain FO cable obtained for twelve load increments applied in a static loading test on the CFA pile. The small circles show the strains determined at the four VW gage levels for the last load increment (maximum load) applied to the pile. The strains measured by the two systems agree well.

The dashed horizontal lines show the depths of the stiffening rings of the reinforcement cage. The rings were size 6x60 mm and located every 0.97 m along the cage. It can be seen from the graph that a local strain reduction was observed in the FO cable at the locations of stiffening rings. This finding is in agreement with observations of Bersan et al. 2018, who investigated detection of highly localized small strains using a Rayleigh-based interrogation unit, Luna OBR4600. Kania and Sorensen (2018) reported the test setup and compared the two systems.

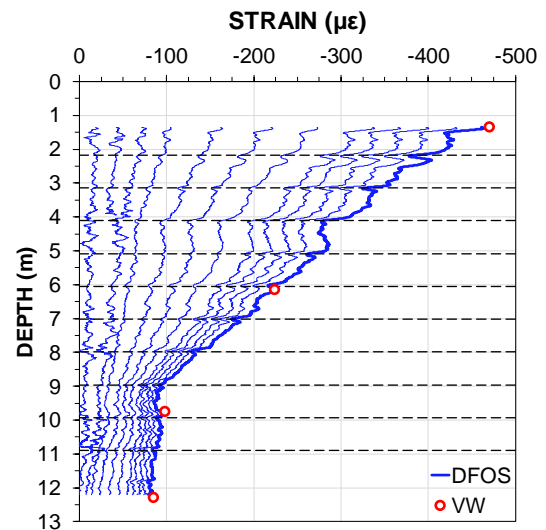


Figure 9 Strain distributions obtained from FO (all load increment) and VW sensors (the last load increment). The dashed, black lines indicate the location of stiffening rings (every 0.97 m)

5.2.2 Influence of cracks in precast concrete driven piles

Cracks and fissures may occur in driven precast concrete piles and even a fissure can distort the FO strain measurements. Figure 10 presents raw strain profiles between 9 and 10.2 m depth obtained from one of the FO strain cables mounted on the side surfaces (c.f., Figure 4b). of one of the precast concrete piles. The strains were measured at the listed selected days after placing the fill. Positive strain values denote compression. As can be seen from the data, numerous peaks of compression and tension appeared along the test pile. The peaks made the smoothing of the strain data difficult. For discussion of the ability to detect cracks in concrete piles using a Rayleigh based IU, see Monsberger et al. (2016)

5.3 Short- and Long-Term Influence of Temperature on Strain Fibre Optic Cables

The temperature considerations are important during short-term (e.g., during the process of pile installation) and long-term measurements for shallow depths where the ground temperature changes seasonally (Alberdi-Pagola 2018). Figure 11 shows the soil temperature on selected days at the test site. The temperature data were recorded from the VW gages installed on one of the driven steel piles. The graph shows that the ground temperature span was about 8 °C at 1 m depth and no more than 0.4 °C at 5.9 m. The temperature at about 10 m depth is equal to the mean annual air temperature at the site. The VW gages mounted on the other test piles indicated similar temperature profiles.

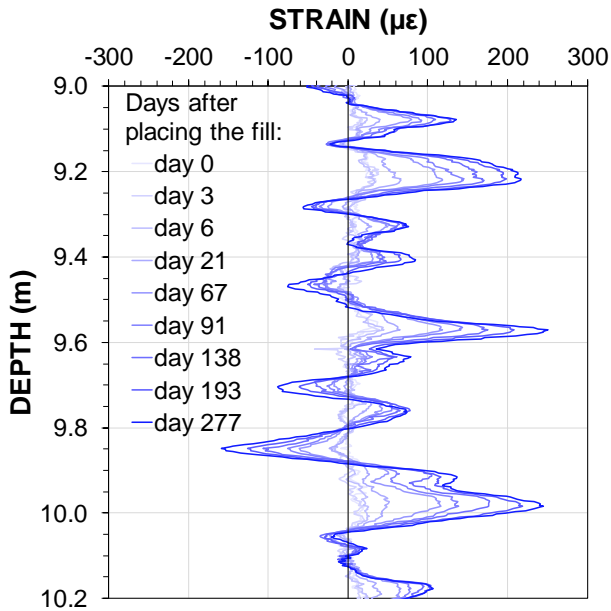


Figure 10 Evolution of cracks along precast concrete pile (raw strain from one of the strain FO cable mounted on the pile)

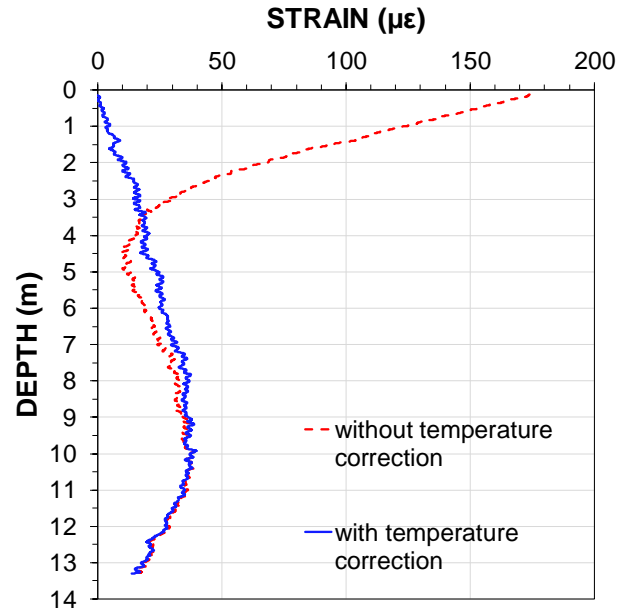


Figure 12 An example of the influence of temperature on the change of strain measured as average of two pairs of FO cables between Sep. 6, 2018 and Jan. 30, 2019

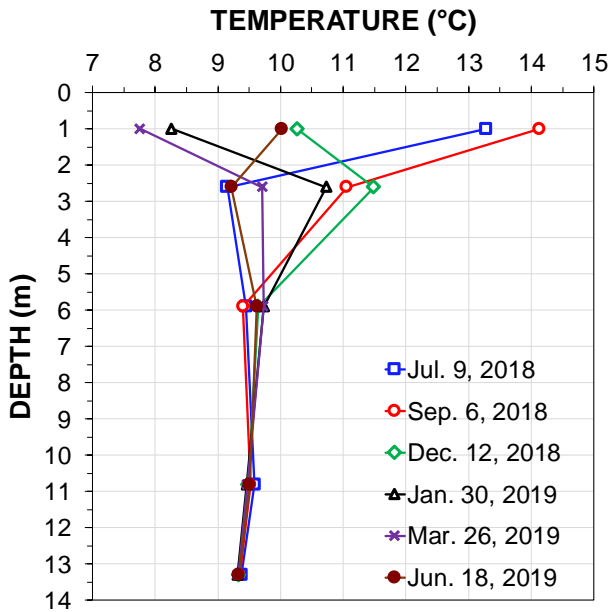


Figure 11 Soil temperature at selected days at the test site

Figure 12 presents the distribution of the average change of strain of two FO cable pairs between September 6, 2018, and January 30, 2019, due to development of negative skin friction, as measured by FO strain cables mounted one of one of the steel piles. The records are shown with and without temperature correction. Positive strain values denote compression of the pile. As expected, a significant temperature correction was needed in the upper part of the pile, where the temperature changed by about 6 °C over initial through the final readings (see Figure 11). Below 9 m depth, the strain distribution with and without the temperature correction are the same, because the seasonal temperature change did not go deeper than that depth at the site (the temperature-corrected curve shows the strain change due to the development of negative skin friction along the pile after placing the fill at the site, resulting in increase of axial strain as the drag force built up and, then, the decrease as the positive shaft resistance reduced the axial force in the pile below a force equilibrium at about 10 m depth).

Figure 13 shows an example of the influence of daily temperature variations on the individual strain FO sensor mounted on the same steel pile. Negative strain values denote elongation of the pile. The initial reading was taken on September 6, 2018 at 06:30h and the figure shows the change of strain at 9:00h and 15:00h. It is very unlikely that mechanically induced strains would have influenced the strain measurements in the test pile during that 8.5-hour period. Therefore, the change above 1.0 m depth is related to temperature changes in the test pile (the spectral shift has changed in the fibre due to both the thermal expansion of steel and the refractive index of the fibre).

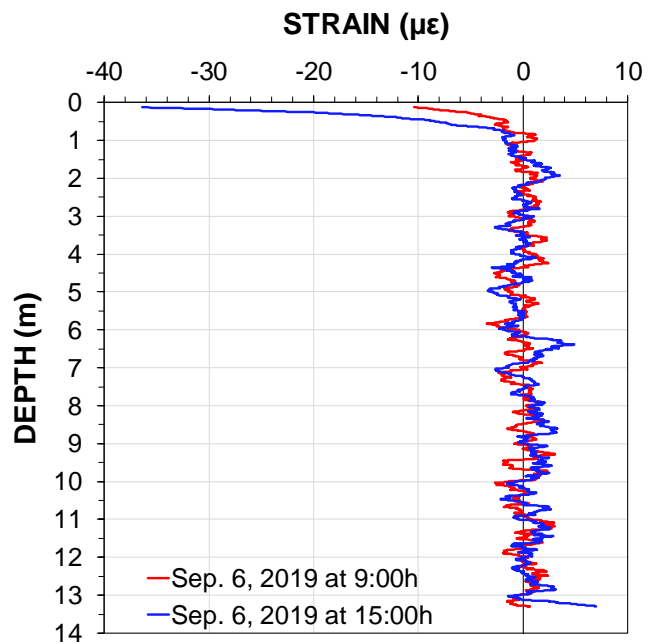


Figure 13 An example of the influence of daily ground temperature changes on the individual FO strain cable on Sep. 6, 2018 from an initial reading taken the same day at 06:30h

5.4 Performance of Gel-Filled Temperature Fibre Optic Cables

Loose tube gel-filled FO temperature cables were installed on the driven piles at the test site. Previous studies have reported the use of loose tube gel-filled FO cables as temperature sensors (Klar et al. 2006, Soga et al. 2015, Pelecanos et al. 2018). However, the findings of the current study show that the loose-tube gel-filled cables installed on driven piles might be influenced by mechanical strains. Figure 14 shows the temperature change between the reference reading recorded on Sep. 6, 2018 and the data recorded immediately after placing the 2.0 m thick fill on Sep. 14, 2018. The presented data were obtained from the VW and temperature FO sensors mounted on the steel test pile. As expected, both opposite mounted VW recorded only small temperature variations at the pile head (at 1.0 m depth) and no temperature change with depth during these 8 days between the reference and the first reading after placing the fill. The temperature change obtained from both opposite mounted VW were in agreement. In contrast, the temperature change profiles obtained from the individual FO temperature cables showed mirrored S-shape curves. Note that an increase and decrease in relative temperature indicates elongation and compression of a FO cable, respectively. The individual FO strain cables mounted close to the temperature DFOS-T0010 and temperature DFOS-T0012 showed similar S-shape compression and elongation respectively with similar S-shape curves. This finding suggests that the gel-filled temperature FO cables, used in this study, were affected by bending of the driven test piles after placing the fill.

5.5 Influence of lateral forces

In order to investigate the influence of lateral forces on a steel driven pile deflected due to one-sided surcharge loading, the data from two individual FO strain cables were compared. To determine the integration coefficients (cf. Eqs. 4 and 5), initial readings were taken after driving a pile and it was also assumed that the pile works as a cantilever beam fixed at the pile toe. Figure 15 shows the strain profiles obtained 126 days after driving the pile from the two individual FO strain cables (S1 and S2). Positive strain values denote elongation (tension). The strain profiles were smoothed using a moving average over 100 strain data spaced every 2.6 mm. Based on the presented strain data the curvature, gradient, and lateral displacement of pile were calculated using the Eqs. 3 - 5.

Figure 16 shows the (a) lateral displacement, (b) the gradient, and (c) the curvature of the steel test pile 126 days after driving. It can be seen from the data that the pile bent due to lateral soil movement at the boundary between the bottom sand layer and the soft soil layer (about 7.5 m depth). The pile head was displaced by about 50 mm.

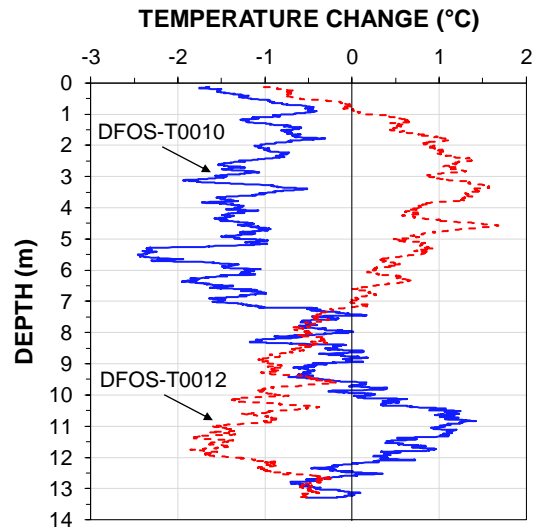


Figure 14 Temperature change obtained from the individual FO temperature cables immediately after placing the fill (Sep. 14, 2018) in reference to the initial reading of Sep. 6, 2018

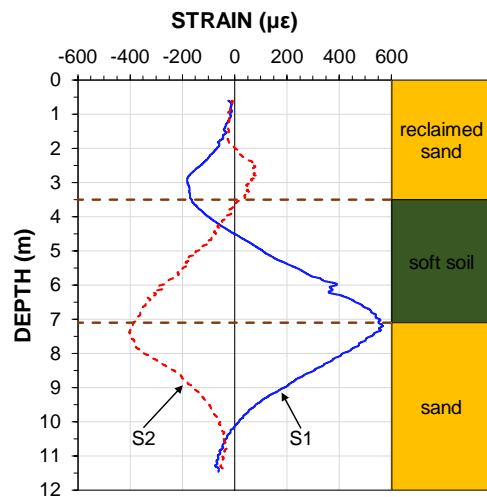


Figure 15 Strain profiles measured in the steel test pile 126 days after driving (the initial reading was recorded immediately after driving the pile)

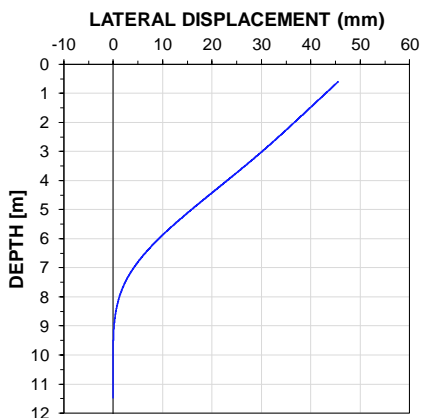


Figure 16 (a) Lateral displacement of the steel test pile recorded 126 days after driving

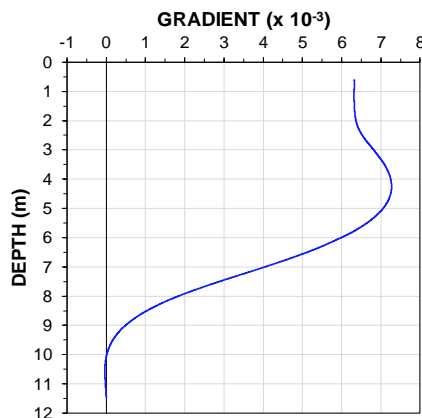


Figure 16 (b) gradient of the steel test pile recorded 126 days after driving

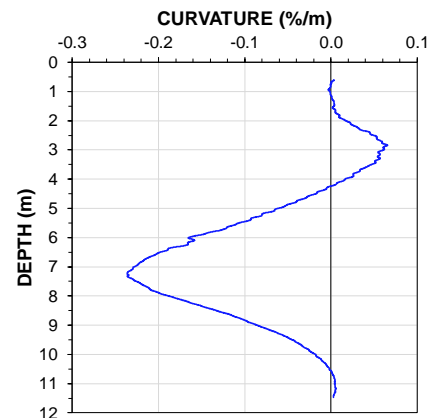


Figure 16 (c) curvature of the steel test pile recorded 126 days after driving

Figure 17 shows the bending moment and shear forces of the test pile due to lateral soil movement from strain change recorded 126 days after driving (the initial reading was recorded immediately after driving the pile). The bending moment and shear force were calculated using the Eqs. 6 and 7, respectively. As recommended by Mohamad et al. (2011), the strain records were smoothed and averaged before differentiation. The moving average was over 200 data points and 2.6 mm length. The shear force acting on the test pile at about 7.5 m depth (the boundary between sand and soft soil layer) was calculated to about 100 kN. Mohamad et al. (2011) highlighted difficulties with estimating shear forces based on the FO strain cable records due to the spatial resolution of the BOTDR analyser used in their study (approximately 1 m spatial resolution spaced every 50 mm). However, as mentioned before, the analyser used in this study had 5.2 mm spatial resolution and 2.6 mm sampling resolution.

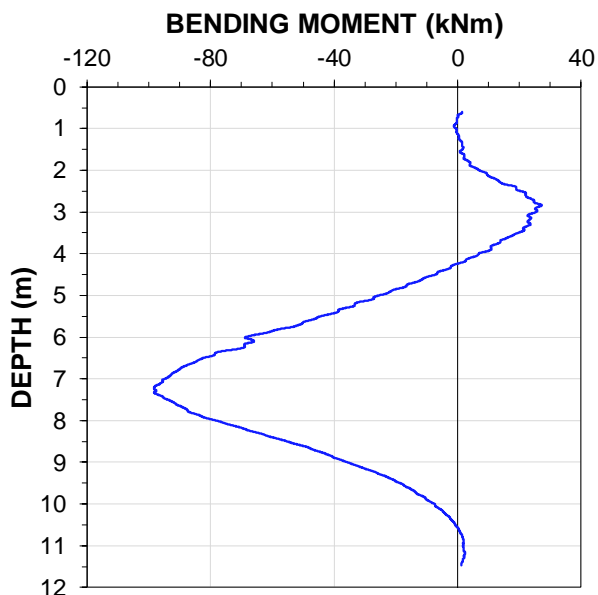


Figure 17 (a) Bending moment diagram

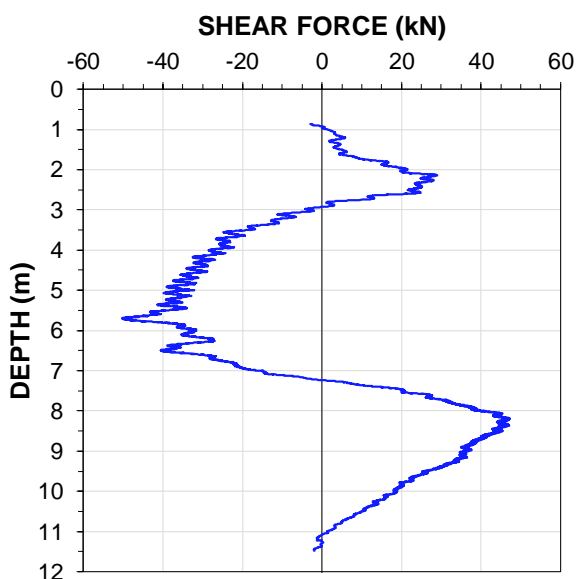


Figure 17 (b) shear force diagram

6. CONCLUSION

Prior studies have reported agreement between VW strain gages and distributed FO strain cables in piles (Mohamad et al. 2017, Pelecanos et al. 2018). This study confirms the agreement between the two instrumentation systems.

FO systems have the advantage over the conventional intermittent measurements (VW strain gages or retrievable extensometers) due to their providing continuous strain and temperature records. The Brillouin-based analysers have the spatial resolution of 0.5-1.0 m and sampling resolution of few centimetres. Such spatial resolution makes it difficult to detect local strain changes, e.g., due to concrete cracks (Zhang and Wu 2008). The Rayleigh-based analyser (Luna ODiSI B) used in this study has the spatial resolution of 5.2 mm and the sampling resolution of 2.6 mm. Therefore, it was possible to detect cracks in concrete (Figure 10) or local changes in pile stiffness (Figure 9).

A temperature change will always affect the FO cable regardless the pile material it is attached to. This is mainly due to temperature dependence of refractive index of the fibre core (Kersey et al. 1997, Luna 2014). In contrast, if the steel vibrating wire (inside a VW strain gage) and the steel or concrete pile has the same thermal expansion coefficient, temperature correction is not needed.

Driven and bored piles can be successfully instrumented with distributed FO cables. The FO cables can be glued directly on the surface or embedded in the piles. Placing the FO cables on the surface of a precast concrete pile will expose the cable to concrete cracks induced during driving.

Distributed FO cables are sensitive to both: temperature and strain changes, therefore, it is necessary to correct the records for temperature changes.

Loose tube gel-filled temperature FO cables used in this study were not suitable for driven piles since they were shown to be sensitive to mechanical strain. Owing to the spatial resolution of the interrogation unit used in this study, it was possible to detect highly localized strain changes due to fissures or change of pile cross section (stiffness).

The data can be smoothed by averaging over time or length. However, with smoothing over length, caution must be applied, as it might disguise local changes.

When two opposite strain FO cables are mounted in a pile, the information about axial and lateral deformation can be obtained. The DFOS can supplement the benefits of inclinometers installed in a pile.

7. ACKNOWLEDGEMENT

The authors would like to thank cp test a/s, Per Aarsleff A/S, Centrum Pæle A/S, DMT Gründungstechnik, GmbH and Innovation Fund Denmark for providing funding for this study and Per Aarsleff A/S for installing the instrumented test piles.

8. REFERENCES

- Alberdi-Pagola, M., 2018. Design and performance of energy pile foundations. PhD thesis. Aalborg University.
- Bersan, S., Bergamo, O., Palmieri, L., Schenato, L. and Simonini, P., 2018. Distributed strain measurements in a CFA pile using high spatial resolution fibre optic sensors. *Engineering Structures*, 160, pp. 554-565.
- Culshaw, B. and Kersey, A., 2008. Fiber-optic sensing: A historical perspective. *Journal of lightwave technology*, 26(9), pp. 1064-1078.
- Fellenius, B.H., 2013. Capacity and load-movement of a CFA pile: A prediction event. *GeoInstitute Geo Congress San Diego*, March 3-6, 2013, Honoring Fred H. Kulhawy—Foundation Engineering in the Face of Uncertainty, ASCE, Reston, VA, James L. Withiam, Kwok-Kwang Phoon, and Mohamad H. Hussein, eds., *Geotechnical Special Publication, GSP 229*, pp. 707-719.
- Fellenius, B.H., 2019. Basics of foundation design—a textbook. Electronic Edition, www.Fellenius.net, 484 p.
- Fellenius, B.H., Kim, S.R., and Chung, S.G., 2009. Long-term monitoring of strain in instrumented piles. *ASCE Journal of Geotechnical and Geoenvironmental Engineering*, 135(11), pp. 1583-1595.

- Inaudi, D. and Glisic, B., 2010. Long-range pipeline monitoring by distributed fiber optic sensing. *Journal of Pressure Vessel Technology*, 132, 011701.
- Kania, J.G. and Sørensen, K.K., 2018. A static pile load test on a bored pile instrumented with distributed fibre optic sensors. 10th International Symposium on Field Measurements in Geomechanics. Rio de Janeiro.
- Kechavarzi, C., Pelecanos, L., and Soga, K., 2019. Distributed fibre optic sensing for monitoring reinforced concrete piles. *Geotechnical Engineering Journal of the SEAGS & AGSSEA*, 50(1).
- Kechavarzi, C., Soga, K.B., Battista, N.D., Pelecanos, L., Elshafie, M.Z.E.B., Mair, R.J., 2016. Distributed fibre optic strain sensing for monitoring civil infrastructure - a practical guide, ICE Publishing, London, UK, 264p.
- Kersey, A.D., Davis, M.A., Patrick, H.J., Leblanc, M., Koo, K., Asking, C., Putnam, M., and Friebele, E.J., 1997. Fiber grating sensors. *Journal of lightwave technology*, 15, pp. 1442-1463.
- Klar, A., Bennett, P.J., Soga, K., Mair, R.J., Tester, P., Fernie, R., St John, H.D., and Torp-Peterson, G., 2006. Distributed strain measurement for pile foundations. *Proceedings of the Institution of Civil Engineers-Geotechnical Engineering*, 159, pp. 135-144.
- Kreger, S.T., Gifford, D.K., Froggatt, M.E., Soller, B.J., and Wolfe, M.S., 2006. High resolution distributed strain or temperature measurements in single-and multi-mode fiber using swept-wavelength interferometry. *Optical Fiber Sensors*. Optical Society of America, ThE42.
- Luna Inc., 2014. Distributed Fiber Optic Sensing: Temperature Compensation of Strain Measurement. Internal report.
- Luna Inc., 2017. ODiSI B. Data sheet.
- Mohamad, H., Bennett, P., Soga, K., Mair, R., and Bowers, K., 2010. Behaviour of an old masonry tunnel due to tunnelling-induced ground settlement. *Géotechnique*, 60(12), pp. 927-938.
- Mohamad, H., Soga, K., Pellew, A., and Bennett, P.J., 2011. Performance monitoring of a secant-piled wall using distributed fiber optic strain sensing. *ASCE Journal of Geotechnical and Geoenvironmental Engineering*, 137(12), pp. 1236-1243.
- Mohamad, H., Tee, B.P., Chong, M.F., and ANG, K.A., 2010. Investigation of shaft friction mechanisms of bored piles through distributed optical fibre strain sensing. 19th International Conference on Soil Mechanics and Geotechnical Engineering 2017, Seoul.
- Monsberger, C., Woschitz, H., and Hayden, M., 2016. Deformation measurement of a driven pile using distributed fibre-optic sensing. *Journal of Applied Geodesy*, 10(1), pp. 61-69.
- Nöther, N., Wosniok, A., Krebber, K., and Thiele, E., 2008. A distributed fiber optic sensor system for dike monitoring using Brillouin optical frequency domain analysis. *Smart Sensor Phenomena, Technology, Networks, and Systems 2008*. International Society for Optics and Photonics, 6933, pp. 69330T.
- Pelecanos, L., Soga, K., Elshafie, M.Z., De Battista, N., Kechavarzi, C., Gue, C.Y., Ouyang, Y., and Seo, H.J., 2018. Distributed fiber optic sensing of axially loaded bored piles. *ASCE Journal of Geotechnical and Geoenvironmental Engineering*, 144(3), pp. 04017122.
- Ravet, F., Niklès, M., and Rochat, E., 2017. A decade of pipeline geotechnical monitoring using distributed fiber optic monitoring technology. *ASME 2017 International Pipeline Geotechnical Conference 2017*. American Society of Mechanical Engineers.
- Soga, K., Kwan, V., Pelecanos, L., Rui, Y., Schwamb, T., Seo, H., and Wilcock, M., 2015. The role of distributed sensing in understanding the engineering performance of geotechnical structures. *XVI European Conference on Soil Mechanics and Structures*.
- Zhang, H. and Wu, Z., 2008. Performance evaluation of BOTDR-based distributed fiber optic sensors for crack monitoring. *Structural Health Monitoring*, 7(2), pp. 143-156.